Mirror mode structures in the asymmetric Hermean magnetosheath: Hybrid simulations

David Herčík[1,2], Pavel M. Trávníček[3,1], Jay R. Johnson[4], Eun-Hwa Kim[4], and Petr Hellinger[1]

Abstract.

Results of two global three-dimensional hybrid simulations of the solar wind interaction with the Hermean magnetosphere are presented for southward and northward interplanetary magnetic field (IMF) orientations. Important dawn-dusk asymmetries of the Hermean bow shock and magnetosheath are observed depending on the IMF orientation. For the southward IMF the dawn side has a thicker magnetosheath with higher β values and slower bulk velocities compared to the dusk side whereas for the northward IMF the dusk side has a thicker and higher β magnetosheath with slower bulk velocities. Mirror mode activity consequently appear at the dawn side for the southward IMF and at the dusk side for the northward IMF. A mechanism for the bow shock and magnetosheath asymmetries is proposed and discussed in the context of the Hermean and terrestrial magnetosheaths.

1. Introduction

Mercury's intrinsic magnetic field was originally observed by Mariner 10 [*Ness et al.*, 1975] and recently confirmed by MErcury Surface, Space ENvironment, GEochemistry, and Ranging (MESSENGER) spacecraft measurements [*Anderson et al.*, 2008]. The current estimate of the Hermean magnetic dipole moment ≈ 190 nTR_M^3 [*Anderson et al.*, 2011] (where R_M is the Hermean radius), so that its strength is about 2×10^3 times weaker than the Earth's dipole moment. Although the Hermean magnetic field is weak, its interaction with the solar wind results in a magnetospheric structure qualitatively similar to the terrestrial magnetosphere [*Slavin et al.*, 2008]. Thanks to many missions aimed to investigate Earth's magnetosphere and together with missions to study large magnetospheres of outer planets, many observations and studies of the magnetosheath have been carried out. The terrestrial magnetosheath is a region with enhanced fluctuations, instabilities, and wave activity resulting from various sources. The solar wind itself is usually a source of low frequency waves. Density variations, Co-rotating Interaction Regions (CIRs), or other sudden discontinuities in the solar wind flow cause bow shock pulsations which are then convected with plasma into the magnetosheath [*Yumoto*, 1988].

Quasi-parallel bow shock and adjacent foreshock region is another source of magnetosheath waves. Particles reflected from the bow shock travel backwards into the solar wind upstream region in the form of a beam which is the source of free energy, that is converted into various waves [*Russell and Hoppe*, 1983]. These waves are then convected back into the magnetosheath [*Krauss-Varban*, 1995]. A quasi-perpendicular bow shock is the source of waves on itself. As the shocked plasma is heated preferably in the direction perpendicular to ambient magnetic field, temperature anisotropy increases. This pressure anisotropy is a source of free energy for ion cyclotron and mirror waves. Another source of waves is the magnetopause which could generate waves as well [*McPherron*, 2005]. At the magnetopause, compressions also efficiently excite kinetic-scale shear Alfvén waves through mode conversion in the strong Alfvén velocity gradient [*Johnson and Cheng*, 1997b]. Kinetic Alfvén waves lead to significant plasma transport and heating [*Johnson and Cheng*, 2001; *Chaston et al.*, 2008]. The magnetopause region is also favourable to Kelvin-Helmholtz instability, due to high velocity shear. Kelvin-Helmholtz instability then can generate magnetosheath waves for large Mach numbers [*Miura*, 1992] when the compressional mode energy can leak away from the shear layer [*Taroyan and Erdélyi*, 2002]. Finally, processes inside the magnetosheath itself produce conditions favourable for generation of waves, such as plasma flow diversion and field line draping effects described by *Zwan and Wolf* [1976].

Properties of the magnetosheath plasma and the corresponding wave activity depend on the parameters of the solar wind especially on the shock Mach number as well as on the angle between shock normal and the interplanetary magnetic field (IMF) – Θ_{Bn}. In particular, the temperature anisotropy $T_\perp/T_\parallel$ (where $T_\perp$ and $T_\parallel$ is the plasma temperature in the perpendicular and parallel directions with respect to the local magnetic field $\boldsymbol{B}$, respectively) decreases as Θ_{Bn} becomes less oblique [*Ellacott and Wilkinson*, 2007]. The temperature anisotropy is a source of free energy, which is released in the form of several types of waves. At the magnetopause, the field line draping produces perpendicular (with respect to the local magnetic field) compression producing the temperature anisotropy $T_\perp > T_\parallel$ that is most significant in the plasma depletion layer.

The magnetosheath waves have been investigated during studies based on data from various missions. For example, data from ISEE 1 and 2 has been analysed by *Hubert et al.* [1998], who suggests that different wave modes appear in the magnetosheath depending on the position in the magnetosheath. Successively from the bow shock to the magnetopause following modes have been identified, compressive and Alfvén ion cyclotron (AIC) mode, pure AIC,

[1]Astronomical Institute & Institute of Atmospheric Physics, Academy of Sciences of the Czech Republic (AsI, ASCR)

[2]Faculty of Nuclear Sciences and Physical Engineering, Czech Technical University, Prague, CR

[3]Space Sciences Laboratory, University California Berkeley, USA

[4]Princeton Plasma Physics Laboratory, Princeton University, Princeton, NJ, USA

0148-0227/12/$9.00

mixed AIC and mirror mode, and pure mirror mode near the magnetopause. Pure mirror modes in isotropic plasma have zero real frequency ($\omega_R = 0$), however, modes with a non-zero real frequency have also been seen near the magnetopause where the real frequency is associated with plasma gradients [*Johnson and Cheng*, 1997a]. The most significant and abundant waves observed in the magnetosheath are AIC and mirror modes, which are generated for sufficiently large $T_\perp/T_\parallel > 1$. AIC and mirror instabilities usually compete with each other for wide range of plasma parameters. Which one of these modes is the major contributor at particular magnetosheath position depends on particular conditions, such as the value of plasma β (ratio between the particle and magnetic pressures) or the particular composition of plasma [e.g., presence of alpha particles, cf., *Gary et al.*, 1993]. Summary of this subject can be found, for example, in *Lacombe and Belmont* [1995] or *Schwartz et al.* [1996].

Mirror waves and related temperature anisotropy driven instability has been reported already in 1960's by [*Barnes*, 1966; *Hasegawa*, 1969] and it has been studied increasingly recently, analysing data from space missions. Mirror instability and waves have been extensively studied theoretically, e.g.[*Kivelson and Southwood*, 1996; *Kuznetsov et al.*, 2007], via numerical simulations [*Califano et al.*, 2008; *Hellinger et al.*, 2009] as well as using satellite observations. The mirror mode has been reported in the Earth's magnetosheath using data from various missions [e.g. *Tsurutani et al.*, 1982; *Fazakerley and Southwood*, 1994; *Walker et al.*, 2002; *Tatrallyay et al.*, 2008]. Beside the Earth's magnetosheath, mirror waves were observed and studied in magnetosheaths of outer planets [*Violante et al.*, 1995; *Bavassano-Cattaneo et al.*, 1998; *Joy et al.*, 2006]. Mirror modes are also observed in the heliosheath downstream of the termination shock [*Tsurutani et al.*, 2011].

Mirror instability is a kinetic instability at fluid spatial scales [*Hasegawa*, 1969]. This instability results from the Landau (transit time) resonance of particles around $v_\parallel = 0$ with a nonpropagating mirror mode [*Southwood and Kivelson*, 1993], i.e., wave mode in a homogeneous plasma, where the mirror wave is a standing wave in the plasma rest frame (zero real part of the wave frequency). In the inhomogeneous medium, drift terms appear in the frequency and the mirror mode becomes propagating. Assuming cold electrons and hot protons the threshold condition for bi-Maxwellian protons is

$$\Gamma = \beta_\perp \left(\frac{T_\perp}{T_\parallel} - 1 \right) - 1 > 0 \qquad (1)$$

(the marginal stability is at $\Gamma = 0$ and plasma is stable with respect to the mirror instability for $\Gamma < 0$). The most unstable mirror mode close to threshold appears for long wavelengths and strongly oblique angles. The most unstable mode of the mirror instability can be estimated using a cold electron approximation [*Hasegawa*, 1969]. For instance the θ_{kB} angle of the most unstable mode is given as

$$\theta_{kB} = \arctan \left(2\sqrt{\frac{\chi}{\Gamma}} \right) \qquad (2)$$

where $\chi = 1 + (\beta_\perp - \beta_\parallel)/2$ [*Hellinger*, 2007]. The mode is strongly compressional with magnetic variations parallel to the ambient magnetic field $\delta B_\parallel$ much larger than the perpendicular ones $\delta B_\perp$. The mirror mode generate nonpropagating wave at the pressure equilibrium, i.e., it leads to the density variations which anticorrelate with the variations of the magnitude of the magnetic field.

While the linear properties of the mirror instability are well known, its nonlinear behaviour is not well understood. Theoretical and numerical studies indicate that different mechanisms (quasilinear diffusion, wave-wave coupling, particle trapping) participate in the nonlinear saturation [*Pantellini et al.*, 1995; *Kivelson and Southwood*, 1996; *Hellinger et al.*, 2009] leading to formation (of wave-trains) of strong pressure-balanced coherent structures in the form of magnetic holes or humps. Fluid modelling [*Passot and Sulem*, 2006] and hybrid simulations [*Trávníček et al.*, 2007b] predict that magnetic humps are typically present when the system is linearly unstable (with respect to the mirror instability) whereas the magnetic holes are typically present in stable regions in agreement with in-situ observations [*Soucek et al.*, 2008; *Génot et al.*, 2009, 2011]. This indicates that the mirror instability generate magnetic humps which evolves to magnetic holes which survive in the mirror-stable plasma.

The global terrestrial and Hermean magnetospheric structures are qualitatively similar but there are important differences. First, the physical dimensions are smaller for Mercury's magnetosphere than for Earth's magnetosphere. The smaller magnetic dipole moment at Mercury leads to a smaller magnetosphere with a magnetopause stand-off distance only about 1.5 R_M depending on the solar wind pressure whereas at Earth the stand-off distance is around 10 R_E, R_M and R_E *are* the Hermean and terrestrial radius respectively. The important parameter for kinetic effects to play significant role is the particle Larmor radius. Taking into account some typical plasma parameters near Earth and Mercury, we can calculate a typical proton Larmor radii. The parameters taken into account as well as the Larmor radius computed for magnetosheath and solar wind conditions at the Earth as well as at Mercury are given in Table 1. The Larmor radius is computed for protons having a temperature typical for given region. The temperature for the Hermean magnetosheath has been taken from estimate given by *Massetti et al.* [2003]. The resulting Larmor radii are examples based on typical plasma parameters expected at various locations to show the different plasma scales. For the magnetosheath plasma conditions the Hermean radius is on the order of ~ 75 Larmor radii. We can compare Larmor radius to the stand-off distance, that express also the magnetic dipole strength of the planet. For magnetosheath conditions at Earth,the stand-off distance ($\approx$10 R_E from the planetary center) is about 1417 Larmor radii. At Mercury the stand-off distance ($\approx$1.5 R_E from the planetary center) is only 114 Larmor radii. This means, that finite Larmor radius effects will play more significant role at Mercury. Local kinetic effects might be also important in global aspects,

Table 1. Typical plasma parameters for the magnetosheath and solar wind conditions at Earth and Mercury.

Parameter	*Units*	*Solar wind*		*Magnetosheath*	
		Earth	Mercury	Earth	Mercury
n	[cm^{-3}]	5	40	15	120
B	[nT]	5	35	20	40
T	[K]	10^5	2×10^5	3×10^5	6×10^5
$v_{\rm sw}$ [a]	[km/s]	400	400	N/A	N/A
v_A [b]	[km/s]	49	120	113	80
r_L [c]	[km]	104	21	45	32
r_L [c]	[R_p] [d]	0.016	0.009	0.007	0.013

[a] $v_{\rm sw}$: solar wind velocity.
[b] v_A: local Alfvén velocity.
[c] r_L: local Larmor radius.
[d] R_p: planetary radius for Earth or Mercury, i.e., 6378 or 2439.7 km respectively.

such as observed e.g. at Mars asymmetry in the magnetosheath flow as reported by *Dubinin et al.* [1998]. Another significant difference is in the time response to any sudden solar wind input and processes in the magnetosheath. The dimensions, lack of ionosphere and stronger solar wind ram pressure *lead* to $\approx$ 30 times faster processes than at the Earth [*Baumjohann et al.*, 2010].

The IMF, which governs the magnetospheric structure and its dynamical response to the solar wind, is in average closer to radial near Mercury compared to the Earth's orbit where the Parker spiral is more tilted and has a significant component in the East/West direction. The Parker spiral angle peaks at $-30°$ and $150°$ at the Hermean orbit (between 0.31 and 0.47 AU) as shown by the statistical study from Helios and MESSENGER data whereas at the Earth's orbit the angle is $-45°$ and $135°$ [*Korth et al.*, 2011]. However, the IMF depends on particular solar wind conditions and the important B_z component of the IMF is varying at both planets and could be either northward or southward. The orientation of IMF B_z also determines the magnetospheric structure, i.e., the location of the foreshock region or the reconnection sites and therefore mass loading into the planetary magnetosphere. These effects seems to be present at Mercury as well.

This paper focuses on mirror modes in the Hermean magnetosheath. Mirror waves are generated by a mirror instability [*Hasegawa*, 1969] which is active for sufficiently strong temperature anisotropy $T_\perp > T_\parallel$. Here are some processes which can generate the anisotropy ($T_\perp > T_\parallel$). First potential source is a quasi-perpendicular bow shock, where the dissipation leads to this temperature anisotropy [*Sckopke et al.*, 1983; *Sckopke*, 1995]. Second possible source of pressure anisotropy is related to changes of the plasma properties due to its flow around the magnetopause [e.g., the field line draping effect, cf., *Tsurutani et al.*, 1982]. Another sources could also generate the temperature anisotropy, e.g., magnetic field and plasma compression.

In this paper we present a detailed analysis of three-dimensional (3-D) hybrid simulations of the interaction between the solar wind and the Mercury focusing on the mirror wave activity in the magnetosheath. First we characterize the equatorial magnetosheath and try to explain observed dawn-dusk asymmetry. Then linked with the asymmetry, we investigate mirror waves in the equatorial region of the magnetosheath. The data also show other regions and sources of mirror waves, that are not studied in detail. It is for example the quasi-perpendicular bow shock, that is source of temperature anisotropy and exhibits favourable condition for mirror wave generation. Mirror waves observed in the equatorial region appear to be generated by the day-side magnetosheath and magnetopause processes.

The paper is organized as follows. In section 2 we present the simulations and data that have been used for the analysis. Global structure of the solar wind - Mercury interaction is then presented with special focus on the dawn-dusk asymmetry. Then mirror wave analysis follows for the two simulation cases. Section 3 discusses some issues raised within the paper and finally section 4 concludes achieved results.

2. Global hybrid simulations

2.1. Model parameters

In this paper we analyse the data from the updated global hybrid simulations based on older datasets introduced in *Trávníček et al.* [2007a], *Trávníček et al. [2009]*, and described in more detail in *Trávníček et al.* [2010]. The model remains similar, however higher resolution, lower downscaling, and dipolar offset is used as described below.

The simulation box coordinates could be denoted as Hermean centric Solar Wind with origin in the Hermean planetary centre, x-direction along the solar wind flow, z-direction along the magnetic axis and y-direction completing the right-hand coordinate system.

We are using a scaled down model of Mercury with a magnetic moment $M = 100,000 B_{\rm sw} d_{p\rm sw}^3 4\pi/\mu_0$, where $B_{\rm sw}$ is the magnitude of the solar wind magnetic field, $d_{p\rm sw} = c/\omega_{pp\rm sw}$ is the proton inertial length in the solar wind, c is the speed of light, $\omega_{pp\rm sw}$ is the solar wind proton plasma frequency. The scaling is necessary due to a limited computation resources. Real Mercury would need larger simulation box to maintain current resolution, which is not possible to achieve with available computation power we have. The solar wind magnetic field $B_{\rm sw}$ corresponds to 20 nT. The $d_{p\rm sw}$ is equivalent to Larmor radius of proton with Alfvén speed $d_{p\rm sw} \equiv v_{A\rm sw}/w_{gp\rm sw}$, where $v_{A\rm sw}$ is the Alfvén speed in the solar wind and $w_{gp\rm sw}$ is the proton gyro-frequency in the solar wind. The downscaling preserves a stand-off magnetopause distance $R_{\rm mp}$ predicted from the pressure balance between the solar wind ram pressure $P_{\rm ram,sw}$ and the magnetospheric pressure: $R_{\rm mp} = [B_{\rm eq}^2/(2\mu_0 P_{\rm ram,sw})]^{1/6} R_M$, where $B_{\rm eq}$ is the magnetic field at the equator of the planet and before downscaling corresponds to 195 nT. Following recent observation of MESSENGER [*Anderson et al.*, 2011], the dipolar magnetic field is shifted towards the north pole by 0.2 R_M. The scaled down radius R_M always remains much larger than the local proton Larmor radius. As shown in Table 1, the planetary radius R_M is ~ 111 (~ 76) Larmor radii for solar wind (magnetosheath) plasma respectively. The scaling factor in these simulations is 1.9, that means the planet will remain an obstacle for the solar wind having radius of several local Larmor radii.

For the simulations here we use a 3-D simulation box with $940 \times 400 \times 400$ mesh points distributed equidistantly along the three (Cartesian) dimensions with the spatial resolution $\Delta x = 0.4\, d_{p\rm sw}$, $\Delta y = \Delta z = d_{p\rm sw}$. The planetary radius is $R_M = 21.727 d_{p\rm sw}$, which gives $17.3 \times 18.4 \times 18.4$ R_M spatial resolution, taking into account one cell dimensions of $0.4 \times 1.0 \times 1.0$ $d_{p\rm sw}$. The simulated planet centre is located at the distance 5.19 R_M in the solar wind flow direction. Macro-particles are advanced with the time step $\Delta t = 0.02\, \omega_{gp\rm sw}^{-1}$, where $\omega_{gp\rm sw}$ is the solar wind proton gyrofrequency; whereas the electromagnetic fields are advanced with the finer time resolution $\Delta t_B = \Delta t/20$.

The magnetic field is initialized with a superposition of the homogeneous IMF $\boldsymbol{B}_{\rm sw}$ and a dipolar planetary magnetic field $\boldsymbol{B}_M$. The IMF $\boldsymbol{B}_{\rm sw} = (B_x, 0, B_z)$, $B_{\rm sw} = 1$, makes an angle $\varphi = \pm 20°$ with respect to the $+X$ axis (i.e., with respect to the solar-wind flow direction) in the plane (X, Z). Here we refer to the simulation with northward IMF ($\varphi = 20°$) as NIMF and to the simulation with southward IMF ($\varphi = -20°$) as SIMF.

At $t = 0$ the simulation box is loaded with 70 macro-particles in each cell outside the planet for both simulations NIMF and SIMF, representing the solar wind Maxwellian isotropic protons with the density $n_p = n_{p\rm sw}$ and the bulk speed $\boldsymbol{v}_p = (4 v_{A\rm sw}, 0, 0)$. This plasma flow is continuously injected from the left boundary of the simulation box at $X = -5.19 R_M$. The ratio of proton to magnetic pressure in the solar wind is $\beta_{p\rm sw} = 1$.

At boundaries, we use open boundary conditions, i.e., macro-particles freely leave the simulation box on all sides. Macro-particles hitting the planetary surface (set at $R_M = 21.727\, d_{p\rm sw}$) are removed from the simulation. We keep $\partial \boldsymbol{B}/\partial t = 0$ in the interior of the planet and $\partial \boldsymbol{E}/\partial r = 0$.

The simulation unit settings corresponds to condition of slow solar wind with speed ~ 450 km/s and density of 15 cm^{-3}.

2.2. Global structure of the interaction

The general structure of the solar wind interaction with the Hermean magnetosphere with its various features has been described in [*Trávníček et al.*, 2010]. The simulated data are also in good qualitative agreement with MESSENGER measurements. Analysis showed typical terrestrial-like magnetosphere with bow shock ahead of the planet, magnetosheath with plasma flowing around the planet along the magnetospheric boundary - the magnetopause. The inner magnetosphere exhibits a plasma belt around the planet, that is connected to the current sheet in the tail region.

Two cases has been studied and presented: northward and southward IMF. One clear distinction for the two cases is the location of the quasi-parallel and quasi-perpendicular bow shock, which causes magnetosheath asymmetry (north-south in case of IMF in meridian plane). Quasi-parallel bow shock is an active region, with turbulent magnetosheath and adjacent foreshock. In the foreshock region wave activity rises, due to backscattered ions from the bow shock interacting with incoming solar wind. In contrast, the quasi-perpendicular bow shock is a quasi-laminar strong and well defined shock boundary, that generates temperature anisotropy. The free energy in the anisotropy is then converted to ion cyclotron waves travelling into the magnetosheath. In particular for southward IMF, the foreshock region is located in the northern part of the bow shock, where the IMF is parallel to the shock normal. Due to the low angle (20°) of the IMF to the solar wind flow, the quasi-perpendicular shock is in the southern part further from the sub-solar line at the flank.

The B_z component of IMF, and especially its direction, affects the overall magnetospheric structure. For southward IMF (SIMF), the magnetosphere is open, which means, that reconnection of IMF and magnetospheric magnetic field lines takes place ahead of the planet and solar wind in the reconnection region can directly enter the magnetopause, that leads into higher total pressure in the magnetosphere and widened magnetospheric tail. On the northern part of the day-side magnetopause the IMF fieldlines reconnect to Hermean magnetospheric fieldlines and are then convected with the magnetosheath plasma flow towards the tail. The northern magnetospheric lobe also exhibits certain plasma density, as the solar wind penetrates along the fieldlines into the magnetospheric region.

In the northward IMF (NIMF) case, the magnetosphere is 'closed' and the field lines are bent along the magnetopause. Reconnection could take place in the southern tail lobe region and in the polar cusps.

As presented, and as expected, the different IMF orientation (opposite B_z component) leads to north-south asymmetry in the foreshock region location. Different magnetic field topology however also leads to significant differences in the magnetospheric structure as described below in respect to dawn-dusk magnetosheath.

2.3. Magnetosheath

In the present analysis we focus on the magnetosheath region. For the analysis purposes, we have prepared fitting procedure to obtain bow shock (BS) and magnetopause (MP) boundary locations and magnetosheath thickness. We have investigated different approaches, i.e. minimum variance analysis, pressure balance, however presented fitting seems to be most robust for the simulated dataset.

We have fitted the dayside magnetosheath at the magnetic equatorial plane to be able to select magnetosheath data only. The boundary detection method is based on 1D data processing. The proton current density is used as an indicator of the magnetopause. Data are acquired along a virtual trajectory from the planetary surface across the magnetosheath, in order to locate the MP position. Then the current density profile is fitted to a tanh function using the least square method. The inflection point indicates the MP location. For the bow shock a similar approach is adopted, similar to *Bale et al.* [2003]. Here, we use the same trajectory for locating the MP but truncated only to points from the MP position further from the planet. This time density data along this trajectory are used for the fit (also with tanh function). Again an inflection point indicates the boundary location. The method however does not provide fully automatic procedure and at some critical points (not sharp enough transition, pre and post boundary oscillations, etc.) need manual correction.

Figure 1 shows the bow shock and magnetopause boundary locations on the dayside magnetosheath at the magnetic equatorial plane, where the magnetic equatorial plane is defined as the plane parallel to geographic equator shifted by 0.2 R_M towards the north pole. This shift stems from the offset of the dipolar field of Mercury observed by MESSENGER [*Anderson et al.*, 2011] and implemented in our simulations. Figure 1 presents comparison of two IMF cases (southward panel a) and northward panel b)). The main feature, we will focus at first, is the apparent asymmetry in magnetosheath geometry, that is connected to asymmetric plasma flow.

2.4. Dawn-dusk asymmetry

IMF orientation drives the structure of the magnetosphere, i.e. foreshock or reconnection position that presents certain asymmetry. The magnetosheath exhibits asymmetry also in the equatorial plane, i.e. the plane with normal parallel to the IMF orientation. The differences can be seen in the equatorial plane comparing dawn and dusk regions of the magnetosheath. In case of SIMF the dawn magnetosheath is thicker, with lower density and magnetic field intensity than on the dusk side. In contrast, in the NIMF case, the dawn magnetosheath exhibits higher density and magnetic field intensity, while the duskside magnetosheath is wider. For comparison see Figure 1 with density data in color where the bow shock and magnetopause are indicated by red and green lines respectively. The data are plotted in the magnetic equatorial plane. White lines represent plasma flowlines and black dashed lines show virtual paths through data across the magnetosheath at the dawn, dusk, and subsolar regions.

Figure 2 shows data along these three paths, that are in the magnetic equator plane (panel a) for trajectory 1S, b) for 2S, and c) for 3S). It shows density, magnetic field, and total pressure (magnetic + plasma) profiles. Yellow fit of the density data is over-plotted. The fit has been done via least square fitting on the following function:

$$f = C_1 \tanh(C_2 x + C_3) + C_4 \tanh(-C_5 x + C_6) + C_7 \quad (3)$$

Where x is the position along the path density and C_1 to C_7 are indexes to be found. The figures indicate the density fit with a yellow line, the location of the bow shock by a green vertical line, and the location of the magnetopause by a vertical blue line. Dashed lines indicate bow shock and magnetopause width estimated based on the fitted curve. For the location estimate of the bow shock *ratio* of parameters C_3/C_2 has been used, as it indicates the shift of the tanh function in the x-axis. The inflection point of the curve is used as the location proxy of the bow shock. Similarly magnetopause position is estimated from indexes C_6/C_5.

Already in the Figure 1, clear differences in the bow shock position can be seen. For southward IMF (panel a)), the bow shock is shifted towards dawn and for northward (b)) towards dusk side. A noticeable difference is also at the magnetopause position, where at the SIMF case the standoff distance is significantly shifted planet-ward, being around 0.3 R_M from the planetary surface. For northward orientation, the stand-off distance is approximately 0.7 R_M. The

Table 2. Comparison of dawn and dusk average values for basic plasma parameters.

Parameter	*Units*	SIMF		NIMF	
		DAWN	DUSK	DAWN	DUSK
n_p	$[n_{p\mathrm{sw}}]$	2.74	2.62	2.7	2.4
B	$[B_{\mathrm{sw}}]$	2.17	2.30	2.54	2.22
β	[ ]	2.30	1.66	1.08	1.85
T	$[T_{\mathrm{sw}}]$	1.97	1.67	1.29	1.9
v	$[v_{\mathrm{sw}}]$	1.87	2.63	2.63	2.26

Values are averages from magnetosheath region in the magnetic equator plane for $y > 0$ for dawn and $y < 0$ for dusk region

smaller stand-off distance for southward IMF results from magnetopause erosion via low latitude reconnection, that has higher rate than in case of northward IMF.

Figure 2 displays the observables across magnetosheath and provides a more detailed view on the magnetosheath thickness that we define by distance from the bow shock to the magnetopause crossing along path normal to the bow shock boundary. It shows also estimated widths of bow shock (BS) magnetopause (MP) and magnetosheath (MS). The fitting procedures *have* its limitations and in some cases produce non-satisfactory results, as in case of 2S trajectory. This is caused by the shape of density profile along the trajectory, with high density pile up just ahead of the magnetopause comparing the bow shock ramp. Therefore *for the fit it appears* more as a peak near the magnetopause and the bow shock jump as a fluctuation only. Here the bow shock width value is not representative.

We have used the fitted bow shock and magnetopause (as indicated in Figure 1) to define the magnetosheath region and compute various observables in the dawn and dusk region separately. The dawn region is defined as magnetosheath region for $y > 0$ and dusk region for $y < 0$. Computed values for the magnetic equatorial plane are given in Table 2.

For SIMF the dusk region exhibits higher average magnetic filed intensity, lower β, lower proton temperature, and significantly higher plasma flow velocity and vice versa for the case of NIMF. This asymmetry is probably affected by two main aspects - magnetosheath thickness and magnetosheath plasma flow.

The magnetosheath thickness is related to the bow shock (BS) shape. In the ideal symmetric case, the bow shock is axis-symmetric and the magnetosheath is therefore also symmetric. What properties and magnetospheric processes cause the bow shock to be asymmetric? First, processes at the bow shock itself might play significant role, but also a magnetosheath flow, its direction and velocity might also influence the bow shock.

At the bow shock, some of the ions are reflected at the shock front and accelerated by the solar wind convective electric field (E_c). These particles could gain up to twice their original energy [*Baumjohann and Treumann*, 1996] and due to gyro-motion hit again the bow shock. The solar wind dissipates the energy by these particles. When looking at the geometry, the gyration orientation might imply some asymmetric aspects, in case the Larmor radius is not negligible. For illustrative purposes to understand the origin of the asymmetry, we refer to Figure 3. First consider the SIMF case shown on panel a). The sketch shows the situation with southward interplanetary magnetic field, that implies a duskward convective electric field. The purple line indicates the symmetric (ideal) bow shock with stagnation point indicated by purple marker (SP_S). When looking at the gyration motion on the dawn side, reflected protons travel shorter paths and could gain less energy than on the dusk side of the bow shock. Therefore, the amount of energy dissipated on the dawn side is lower than on the dusk side. In order to increase the dissipation energy on the dawn side the change of geometry is necessary. Via shift of the bow shock stagnation point dawn-ward, the shock Mach number increases, due to the change of the normal of the bow shock. The normal vector of the bow shock at particular point increases its sun-ward component, which hence increases shock Mach number. The normal component of the reflected proton at this particular position is increased, in respect to original bow shock shape, and therefore the dissipation of the energy becomes higher. On the dusk side same mechanism cause decrease in the dissipation and the balance of the dissipation on both sides (dawn and dusk) is achieved. As a result, the bow shock shape changes and the stagnation point shifts towards dawn. For northward IMF the situation is vice versa because the gyration switches direction. The situation is sketched on panel b) of Figure 3.

Proposed hypothesis is one of possible explanations of the primary source of the mechanism. Most likely, the kinetic effects will play significant role in the mechanism, but additionally other effects on the bow shock and behind will probably contribute to the asymmetry as well as the flow within the magnetosheath itself.

The shape of the bow shock implies the magnetosheath flow. In particular the angle between solar wind direction and the bow shock normal affects the velocity direction change behind the shock. Behind the shock, there is a change in tangent (to the bow shock) component of the velocity in order to bend the flow around the obstacle. At the stagnation point, precisely, the flow should be not diverted. On either sides of the stagnation point, the flow deviates in opposite directions. The estimation on the tangent component magnitude can be derived from Rankine-Hugoniot conditions [*Zwan and Wolf*, 1976, cf.].

The bow shock asymmetry previously discussed implies a shift in the stagnation point. In other words, the location of the bow shock, where the shock normal is anti-parallel to the solar wind flow, shifts towards dawn in SIMF case as indicated by red marker (SP_A) in Figure 3 panel a).

Hence the flow diverts asymmetrically along the planet, but more solar wind plasma flow towards dusk side of the magnetosheath (for SIMF case). Due to the bow shock shift, magnetosheath thickness at the dusk region is lower than on the dawn side resulting in a faster magnetosheath plasma flow.

This initial flow pattern applies near the bow shock; however, in the inner magnetosheath other effects could play role in the flow asymmetry. One of the candidates is grad B drift. It switches direction based on the magnetic field direction. One could expect the magnetic field increasing towards the magnetopause by a so called draping effect resulting in a magnetic field gradient pointing towards magnetopause. The drift velocity would then contribute to the flow in the duskward direction in case of SIMF. However, when studying the magnetosheath in detail, the magnetic field is highly variable when going from the bow shock to the magnetopause. The resulting drift speeds does not appear to have collective behaviour, that would contribute to the general magnetosheath flow. In the case of SIMF, magnetic merging might lessen the draping effect significantly. However even in the NIMF, the magnetic field also varies significantly, not allowing global magnetic field gradient direction.

Although the magnetic field gradient is not adequate to account for the asymmetry, the total pressure gradient, i.e. plasma plus magnetic field pressure, seems to rise steadily (in average) towards the magnetopause. Examples of the total pressure data acquired from the simulation data along subsolar path in the dayside magnetosheath are shown in Figure 2 on all panels for different magnetosheath crossings. This gradient would cause diamagnetic current to be directed duskward (dawnward) in SIMF(NIMF) case respectively. However, the resulting plasma behaviour is complex with contributions from the various drifts.

The sum of the afore mentioned aspects, that are dependent on the IMF direction, act in unison towards thinner magnetosheath and faster plasma in dusk region for SIMF and dawn region for NIMF.

Is there some further effect of the asymmetry of the magnetosheath flow and properties further in the magnetosheath? We have investigated the wave activity in respect to the mirror waves comparing the two sides (dawn/dusk) of the magnetosheath.

2.5. Mirror mode identification

A good indicator of the mirror mode activity is an anticorrelation between the magnetic field B and the proton density n_p fluctuations. It does not however grant a unique mode identification and several other methods exist in [cf., *Schwartz et al.*, 1996]. We have computed (Pearson) correlation coefficient between the proton density and magnetic field $\langle n_p, B\rangle$ from simulated data using 125 nearest space points.

As the anticorrelations provide necessary but not sufficient indicator of the mirror wave activity we have looked at other properties of the mirror waves. These are plasma beta and mirror mode instability threshold. As a final confirmation, the spatial Fourier analysis has been made.

2.5.1. Results for Southward IMF

We will first focus on the simulation SIMF with southward IMF. As stated above, the first indicator for mirror waves that we examine is the enhanced anticorrelation of density and magnetic field. The computed correlations for both simulations are shown in Figure 4. Figure 4 left panel shows correlation $\langle n_p, B\rangle$ in the magnetosheath for SIMF case in magnetic equator plane. For comparison, the right panel shows the same plot for NIMF.

Figure 4 left panel shows that a region of strong anticorrelations occurs near the inner magnetosheath, i.e. in the region further from boundaries - bow shock and magnetopause) at the dawn side of the planet. Ahead of the planetary centre, anticorrelations start to appear near the day-side magnetopause and then are advanced towards the dawn region.

Correlation $\langle n_p, B\rangle$ is high at the bow shock where these two quantities increase simultaneously. In the inner magnetosheath the correlation is mainly characterized by scattered positive values except in the aforementioned dawn region. Close to the magnetopause, the correlations drop to negative values. The inner part of the dawn side of the magnetosheath exhibits anticorrelations all along the magnetotail and the area of anticorrelations broadens together with the magnetosheath thickness itself. There are anticorrelations visible also in the further tail (from approximately 5 R_M behind the planet) in the whole magnetosheath.

The dawn region for SIMF has been found to be thicker with lower plasma flow velocity, higher temperature, and higher β (see Figure 2 and Table 2). High beta conditions are favourable for mirror waves. The conditions for mirror instability to grow are given by the growth factor in equation (1). When looking at the global conditions for mirror mode in case of SIMF, in terms of high Γ, they are favourable for mirror instability growth behind the quasi-perpendicular shock, i.e. in the southern part of the magnetosheath. High Γ values could be found also at the magnetopause behind the quasi-parallel bow-shock, i.e. at the northern part of the magnetosphere. Let us focus however, on the region of interest, the dayside magnetosheath at magnetic equatorial plane, here Γ shows an enhanced (> 0) growth factor near the dawn side magnetopause, while the dusk side (ahead of the planet) exhibits lower values, as shown on Figure 5 panel a). Further behind the planet in the magnetosheath, the Γ value approaches marginal stability.

Based on this preliminary indicator of possible mirror waves, further analysis has been performed in order to investigate region of anticorrelations and possible mirror wave activity. High Γ values on the dawn side indicate the possible growth of the mirror instability, that could lead in mirror waves growth and appearance further downstream in the magnetosheath.

We have acquired data along one selected flowline, that crosses the dawn side at magnetic equator plane. The path is indicated by a black dashed line in Figure 4. Data along the flowline are plotted in Figure 6. The anticorrelations could be seen comparing magnetic field (panel a)) and proton density field (panel b)). However further downstream the density variations are not large and the anticorrelation is not visible clearly at first glance. Just behind the bow shock, mirror mode is unstable $\Gamma > 0$ (panel c)), oscillating around marginal stability further downstream. Proton β ($\beta = n_p K_B T/(B^2/2\mu_0)$) on panel d) also shows high values along the path, another favourable condition fore mirror waves. Moreover β is exhibiting sharp changes: drops and peaks. Such a structure is consistent with anticorrelations of density and magnetic field. High proton density and low magnetic field means high β and on the contrary high magnetic field and low density means low β. Finally panel e) shows temperature anisotropy to be higher than 1 most of the path, that is a source of energy for the mirror instability to *grow* from.

For further analysis we have chosen two areas on the opposite side of the Hermean magnetosheath. One region is located on the dawn (denoted by the black rectangle in Figure 4) and is in the range of coordinates: $x \in (0.3, 1.5)$, $y \in (2.3, 3.8)$, and $z \in (-0.7, 0.7)$. The other on the dusk (white rectangle in Figure 4) side of the planet within coordinates: $x \in (0.3, 1.5)$, $y \in (-3.8, -2.3)$, and $z \in (-0.7, 0.7)$. Data from these regions *have* been used for further analysis in order to highlight the differences of these regions in terms of mirror waves. Average values of β have been computed for the selected regions. For the dawn region $\beta = 3.57$ whereas for the dusk region $\beta = 1.80$, which is consistent with enhanced observations of mirror waves in the dawn region.

As a final confirmation of the mirror waves present in the magnetosheath, we have performed spatial Fourier analysis of the two different regions of the magnetosheath, one dataset is taken from the dawn (expected mirror waves) and the other from the dusk side as indicated in Figure 4 with black rectangle showing selected area for dawn and white rectangle for dusk region.

The analysis has been performed on the two datasets selected from magnetic field simulated data, subtracting the background average field and removing waves with wavenumbers equal to ± 1, that correspond to the dimensions of the box selected for the analysis. Figure 7 shows in arbitrary units normalized magnetic field energy distribution according to the wavevectors in the $k_\parallel$ versus $k_\perp$ plane in four regions. Results from the SIMF simulation are shown for dawn region on panel a) and for dusk region on panel c).

Panel a) displays the results of the analysis taking the data from the dawn region, the one suspected of mirror waves. There is main maxima marked by the star marker corresponding to $\theta_{kB} = 82°$, being the angle between magnetic field B and wavevector, k. Mirror waves propagate perpendicularly or strongly obliquely in respect to ambient magnetic field direction. *Gary* [1992] also showed, that θ_{kB} also depends inversely on the plasma β, so the θ_{kB} shifts from perpendicular direction to lower values with increasing β. According to hybrid expanding box (HEB) simulations by *Trávníček et al.* [2007b], the θ_{kB} for mirror waves is between approximately $60°$ and $90°$. We have computed the theoretical θ_{kB} (in the Equation (2)) for the dawn side at the subsolar region, where the mirror waves likely originate. We have used data from the dawn sub-solar magnetosheath. In particular the data from magnetosheath in the magnetic equator plane have been limited to the region $x \in (-2, 0)R_M$, $y \in (0, 4.5)R_M$. Furthermore, data only from locations, where the mirror mode should be unstable, i.e. $\Gamma > 0$ have been used. Resulting average θ_{kB} in this selected dataset is $64.68°$, which is lower than the maxima in the Fourier analysis marked with a star. However the Fourier analysis result indicates waves with a broader range of θ_{kB} angles. And the theoretical value is an average from the magnetic equator plane only, that might not involve all source locations.

We have also computed the corresponding wavelength [using Eq. (25) of *Hellinger*, 2007] in order to confirm, that the mirror waves would be able to grow within the unstable region of Mercury's magnetosheath. The computed averaged value is $\lambda = 8.7 d_{\rm psw}$. We have used the same selected points as for previous θ_{kB} computation. The magnetosheath dimensions are much larger than this value, and therefore, the local theory of instability discussed above is applicable. The corresponding k vector is 0.72, that corresponds to the maxima marked in panel a).

Panel c) shows the results dusk side region, that show different pattern. Quasi-parallel waves could be found in the spectrum, that are more likely ion cyclotron waves. The maximum near zero k value should be accounted for artificial contribution to the spectrum, or probably bow shock crossing, that interferes with the selected region.

It can be concluded, that the mirror instability grows in the day-side dawn magnetosheath region giving rise to mirror waves that are then transported with the plasma flow further down-stream into the magnetosheath.

2.5.2. Results for Northward IMF

For comparison, we have performed the same analysis for the second simulation NIMF with the northward IMF. The computed correlations are shown in Figure 4 panel b). In this case, the anticorrelations appear in the dusk region, i.e., at the opposite position compared with the southward IMF orientation. Similar asymmetry is visible in the Figure 5 panel b), that shows Γ. In contrast to the SIMF simulation, here the enhanced mirror growth regions appears on the dusk side. Also the Fourier analysis confirms the fact that the mirror waves are generated in the magnetic equator near the dusk region (see Figure 7, panel b) for dawn and panel d) for dusk side). The properties and behaviour on the dusk side correspond to the dawn side in simulation SIMF and vice versa. There is therefore a mirror wave source mechanism, that is asymmetric in the magnetosheath and depends on the IMF orientation.

3. Discussion

We have observed magnetosheath asymmetry in the equatorial plane for northward and southward IMF, that is driven by the IMF orientation. The asymmetry appears in the bow shock geometry as well as in the magnetosheath properties. The asymmetry is most probably result of a combination of kinetic effects on the bow shock and drifts in the magnetosheath. *A hypothesis for explanation of the primary driver of the effect has been provided. We believe, that the origin of asymmetry lies in energy dissipation in the dusk and the dawn region generated due to a local geometry of the bow shock and significant Larmor radius. For confirmation of the hypothesis and explanation of further mechanisms that contribute to the effect, detailed study shall be provided comparing enhanced simulations and in-situ data.*

Certainly, the kinetic effect will be significant only in case the Larmor radius, compared to the magnetospheric structure, is not negligible. In the present simulations, we have used the downscaled planet by approximately factor of 1.9. This would increase importance of the kinetic effects. The real Hermean magnetosphere might exhibit less significant asymmetry.

In order to estimate the effect in for real conditions, we have carried a *test particle simulation* for the Earth and Mercury case using *Chao et al.* [2002] model of the Earth's bow shock and similar shape model with adapted parameters for Mercury (with stand-off bow shock distance estimated to 2 R_M). A 2D simulation of the proton specular reflection shows the differences in energies of reflected proton that hits the bow shock second time for the dawn and dusk side of the magnetosphere. Protons has been injected ahead of the bow shock (in X direction -5 R_M for Mercury and -20 R_E for the Earth) at +/- 1 and +/-2 R_M (R_E) for Mercury (Earth) respectively. The *simulation* injects a proton ahead of the bow shock with initial bulk and thermal velocity. Then it proceeds with the trajectory calculation, at the bow-shock specular reflection takes place modifying the normal component of the particle velocity (reversing and multiplying by 2). On the second encounter with bow shock final energy of the incident proton is calculated. Table 3 summarizes the results of the *simulation* with following input parameters: proton bulk speed = 400 km/s, proton thermal speed = 70 km/s, and IMF = 35 nT for Mercury. For the Earth, the parameters are following: proton bulk speed = 400 km/s, proton thermal speed = 50 km/s, and IMF = 5 nT.

For Mercury case, the geometry and conditions result in a situation, where the energy of reflected and accelerated protons, that hit the bow shock for the second time after reflection, is much higher in the dusk region for southward IMF and in dawn region for northward IMF. In particular for Mercury with southward IMF at the distance of $2R_M$ from the subsolar line the energy gain of one proton on the dawn side is 0.7 less than on the dusk side. For the Earth at $2R_E$ from the subsolar the energy gain is only 0.96 times less on the dawn side than on the dusk side.

The effect is general and should take place in all supercritical bow shocks, where reflected ions contribute significantly to the energy dissipation. How significant is the effect, is however dependent on the ratio of magnetospheric to Larmor radius scales.

There is also a question of whether the presented simulations are relevant to real Hermean conditions. The main concern in respect to the kinetic effects on the bow shock is about the shock Mach number and the criticality of the shock as it defines the role and amount of reflected protons on the bow shock.

At Mercury, high variability of shock numbers are to be expected from $M_A \sim 1$ to highly supercritical numbers [*Baumjohann et al.*, 2006; *Clark*, 2007; *Fujimoto et al.*, 2007], as well as the plasma beta that can be from 0.2 to 0.9 [*Fujimoto et al.*, 2007]. Conditions for supercritical shock are as well likely to be observed as for sub-critical. Moreover, even for low Mach numbers and low beta conditions, reflected protons still might be present and play significant role. As *Hellinger et al.* [2002] showed the role of reflected particles is important for a large variety of Mach numbers and plasma beta. In particular Figure 2 in *Hellinger et al.* [2002] shows, that even for beta 0.2 and Mach number 2, the shock is non-stationary and therefore there is a high percentage of reflected ions.

In the presented simulations the Alfvén Mach number on the sub-solar point in the simulations is 4, beta in the solar wind is 0.5. For the magnetosheath the parameters vary, beta have values from below 1 up to 10. Region of suspected mirror waves has high beta conditions. Comparing these values from the simulation to e.g. values mentioned in *Fujimoto et al.* [2007] the Mach number is typically 3.9 and beta is 0.5 at the *perihelion*, which matches the simulation set up.

The dawn-dusk asymmetry in the magnetosheath has been recently observed by MESSENGER in terms of Kelvin-Helmholtz waves. *Sundberg et al.* [2012] reported, the K-H waves appearing in the post-noon and dusk region of

Table 3. Model results of the energy (in eV) gain difference of the bow shock reflected protons. The proton injected at the distance indicated in the table with '+' sign relevant for DAWN and '−' sign for DUSK region.

	Mercury				Earth			
	SIMF		NIMF		SIMF		NIMF	
	+/-1 R_M	+/-2 R_M	+/-1 R_M	+/-2 R_M	+/-1 R_E	+/-2 R_E	+/-1 R_E	+/-2 R_E
dawn [eV]	7271	7066	14114	9846	9850	9688	12845	12257
dusk [eV]	10445	12005	10807	8189	10212	10227	12401	11321
ratio[a]	0.70	0.59	1.31	1.20	0.96	0.95	1.04	1.08

[a] ratio of dawn/dusk energy values

the magnetopause. The asymmetry seen in the simulations might also explain such observations, while the K-H instability is generated for high velocity shear. As shown above, there is quite strong asymmetry in the velocity flow for dusk and dawn region. More detailed study of the K-H behaviour and dependency on the IMF and other conditions will be also part of a future study.

We have reported observed mirror waves at the dawn/dusk side for southward/northward orientation of the IMF respectively, most probably generated near the day-side magnetopause region. However, favourable conditions for mirror waves are found also just behind the quasi-perpendicular shock and near the magnetopause, especially at the magnetopause behind the quasi-parallel bow shock.

4. Conclusions

We have performed a study of the IMF dependence of mirror mode structures in the magnetosheath of Mercury using hybrid simulations. The simulations used for this study and some results of the data analysis have been presented in a previous paper by [*Trávníček et al.*, 2010]. Here we have focused on the dawn-dusk asymmetry feature of the data sets. The asymmetry *seems to be* driven by the IMF orientation and, as we argued, stems from local kinetic processes at the bow shock and combination of drifts in the magnetosheath. The asymmetry appears in magnetosheath parameters and also in the geometry.

We have focused on the mirror waves identified within the Hermean magnetosheath near the magnetic equatorial plane in order to estimate the effect of the asymmetry. First, correlations of ion density and magnetic field magnitude ($\langle n_p, B\rangle$) have been computed. This feature serves as a first indicator of mirror waves because mirror waves exhibit anticorrelations of n_p and B. The correlation values have been computed in the entire simulation box for both simulation cases (SIMF and NIMF). Enhanced anticorrelations were observed in the inner magnetosheath of both simulations, but they occurred in different regions. For the SIMF simulation, there is a region of anticorrelations on the dawn side of the planet. When looking at data from the other simulation, NIMF, the enhanced anticorrelation region appears on the opposite (dusk) side.

We have carried a set of analysis in order to confirm mirror waves to be present. Focusing on the SIMF simulation, on the dawn side there are indicators favouring mirror waves. There is higher average β and region of enhanced mirror mode growth factor Γ on the dawn side than on the dusk side. Final verification of the presence of waves was demonstrated through spectral Fourier analysis. The results have shown significant wave activity in the dawn region and quiet conditions on the dusk side for simulation SIMF. For the second simulation NIMF, the situation is vice versa. The waves appear on the dusk side of the magnetosheath.

Mirror unstable conditions are in the day-side magnetosheath region predominantly on dawn (dusk) side for SIMF (NIMF) respectively. There, where the magnetic field lines are draping ahead of the magnetopause, the plasma β and temperature anisotropy increase giving rise to mirror instability. Then mirror waves starts to grow and transfer the energy with the plasma flow towards the inner magnetosheath.

Further investigation of the magnetosheath asymmetry and comparison with real data obtained by the MESSENGER spacecraft will follow.

Acknowledgments. The research at the Astronomical Institute, ASCR leading to these results has received funding from the European Commission's Seventh Framework Programme (FP7) under the grant agreement SWIFF (project number 263340) and SHOCK (project number 284515), and from Czech Ministry of Education, Youth and Sports under project number ME09009 and project RVO:67985815. At Institute of Atmospheric Physics work was supported by RVO: 68378289. The work at the University California Berkeley was supported by NASA grants NNX11A1164G, NNH06ZDA001N, and NNX12AD08G. The work at the Princeton University was supported by NASA grants (NNH09AM53I, NNH09AK63I, and NNH11AQ46I), NSF grant ATM0902730, and DOE contract DE-AC02-09CH11466.

References

Anderson, B. J., M. H. Acuña, H. Korth, M. E. Purucker, C. L. Johnson, J. a. Slavin, S. C. Solomon, and R. L. McNutt (2008), The structure of Mercury's magnetic field from MESSENGER's first flyby, *Science*, *321*, 82–85, doi: 10.1126/science.1159081.

Anderson, B. J., et al. (2011), The global magnetic field of Mercury from MESSENGER orbital observations, *Science*, *333*, 1859–1862, doi:10.1126/science.1211001.

Bale, S. D., F. S. Mozer, and T. S. Horbury (2003), Density-transition scale at quasiperpendicular collisionless shocks, *Phys. Rev. Lett.*, *91*, 1–4.

Barnes, A. (1966), Collisionless damping of hydromagnetic waves, *Phys. Fluids*, *9*, 1483–1495.

Baumjohann, W., and R. A. Treumann (1996), *Basic Space Plasma Physics*, Imerial College Press, London.

Baumjohann, W., et al. (2006), The magnetosphere of Mercury and its solar wind environment: Open issues and scientific questions, *Adv. Space Sci.*, *38*, 604–609, doi: 10.1016/j.asr.2005.05.117.

Baumjohann, W., et al. (2010), Magnetic field investigation of Mercury's magnetosphere and the inner heliosphere by MMO/MGF, *Planet. Space Sci.*, *58*, 279–286.

Bavassano-Cattaneo, M. B., C. Basile, G. Moreno, and J. D. Richardson (1998), Evolution of mirror structures in the magnetosheath of Saturn from the bow shock to the magnetopause, *J. Geophys. Res.*, *103*, 11,961–11,972.

Califano, F., P. Hellinger, E. Kuznetsov, T. Passot, P. L. Sulem, and P. M. Trávníček (2008), Nonlinear mirror mode dynamics: Simulations and modeling, *J. Geophys. Res.*, *113*, A08219, doi:10.1029/2007JA012898.

Chao, J. K. and Wu, D. J. and Wang, X. Y. and Kessel, M. and Chen, S. H. and Lepping, R. P. (2002), Models for the size and shape of the Earths magnetopause and bow shock, *in Space Weather Study Using Multipoint Techniques*, 127–140.

Chaston, C., et al. (2008), Turbulent heating and cross-field transport near the magnetopause from THEMIS, *Geophys. Res. Lett.*, *35*, L17S08, doi:10.1029/2008GL033601.

Clark, P. E. (2007), *Dynamic Planet: Mercury in the Context of Its Environment*, Springer, New York.

Dubinin, E., K. Sauer, M. Delva, and T. Tanaka (1998), The IMF control of the Martian bow shock and plasma flow in the magnetosheath . Predictions of 3-D simulations and observations, *Earth Planets Space*, *50*, 873–882.

Ellacott, S., and W. Wilkinson (2007), Heating of directly transmitted ions at low Mach number oblique collisionless shocks: A statistical physics formulation, *Planet. Space Sci.*, *55*, 2251–2256.

Fazakerley, A. N., and D. J. Southwood (1994), Mirror instability in the magnetosheath, *Adv. Space Sci.*, *14*, 65–68.

Fujimoto, M., W. Baumjohann, K. Kabin, R. Nakamura, J. A. Slavin, N. Terada, and L. Zelenyi (2007), Hermean Magnetosphere-Solar Wind Interaction, *Space Science Reviews*, *132*(2-4), 529–550.

Gary, S. P. (1992), The mirror and ion cyclotron anisotropy instabilities, *J. Geophys. Res.*, *97*, 8519–8529.

Gary, S. P., S. A. Fuselier, and B. J. Anderson (1993), Ion anisotropy instabilities in the magnetosheath, *J. Geophys. Res.*, *98*, 1481–1488.

Génot, V., E. Budnik, P. Hellinger, T. Passot, G. Belmont, P. M. Trávníček, P. L. Sulem, E. Lucek, and I. Dandouras (2009), Mirror structures above and below the linear instability threshold: Cluster observations, fluid model and hybrid simulations, *Ann. Geophys.*, *27*, 601–615.

Génot, V., L. Broussillou, E. Budnik, P. Hellinger, P. M. Trávníček, E. Lucek, and I. Dandouras (2011), Timing mirror structures observed by cluster with a magnetosheath flow model, *Ann. Geophys.*, *29*, 1849–1860.

Hasegawa, A. (1969), Drift mirror instability in the magnetosphere, *Phys. Fluids*, *12*, 2642–2650.

Hellinger, P. (2007), Comment on the linear mirror instability near the threshold, *Phys. Plasmas*, *14*, 082105.

Hellinger, P., P. M. Trávníček, and H. Matsumoto (2002), Reformation of perpendicular shocks: Hybrid simulations, *Geophys. Res. Lett.*, *29*(24), 29–31, doi:10.1029/2002GL015915.

Hellinger, P., E. A. Kuznetsov, T. Passot, P. L. Sulem, and P. M. Trávníček (2009), Mirror instability: From quasi-linear diffusion to coherent structures, *Geophys. Res. Lett.*, *36*, L06103, doi:10.1029/2008GL036805.

Hubert, D., C. Lacombe, C. C. Harvey, M. Moncuquet, C. T. Russell, and M. F. Thomsen (1998), Nature, properties, and origin of low-frequency waves from an oblique shock to the inner magnetosheath, *J. Geophys. Res.*, *103*, 26,783–26,798.

Johnson, J. R., and C. Z. Cheng (1997a), Global structure of mirror modes in the magnetosheath, *Journal of Geophysical Research*, *102*(A4), 7179–7189, doi:10.1029/96JA03949.

Johnson, J. R., and C. Z. Cheng (2001), Stochastic ion heating at the magnetopause due to kinetic Alfvén waves, *Geophys. Res. Lett.*, *28*(23), 4421–4424.

Johnson, R. E., and C. Z. Cheng (1997b), Kinetic Alfven waves and plasma transpport at the magnetopause, *Geophys. Res. Lett.*, *24*(11), 1423–1426.

Joy, S. P., M. G. Kivelson, R. J. Walker, K. K. Khurana, C. T. Russell, and W. R. Paterson (2006), Mirror mode structures in the Jovian magnetosheath, *J. Geophys. Res.*, *111*, A12212, doi:10.1029/2006JA011985.

Kivelson, M. G., and D. J. Southwood (1996), Mirror instability ii: The mechanism of nonlinear saturation, *J. Geophys. Res.*, *101*, 17,365–17,371.

Korth, H., B. J. Anderson, T. H. Zurbuchen, J. A. Slavin, S. Perri, S. A. Boardsen, D. N. Baker, S. C. Solomon, and M. J. R. L (2011), The interplanetary magnetic field environment at Mercury's orbit, *Planet. Space Sci.*, *59*, 2075–2085.

Krauss-Varban, D. (1995), Waves associated with quasi-parallel shocks: Generation, mode conversion and implications, *Adv. Space Sci.*, *15*, 271–284.

Kuznetsov, E. A., T. Passot, and P.-L. Sulem (2007), Dynamical model for nonlinear mirror modes near threshold, *Phys. Res. Lett.*, *98*, 235003.

Lacombe, C., and G. Belmont (1995), Waves in the earth's magnetosheath: Observations and interpretations, *Adv. Space Sci.*, *15*, 329–340.

Massetti, S., S. Orsini, a. Milillo, a. Mura, E. De Angelis, H. Lammer, and P. Wurz (2003), Mapping of the cusp plasma precipitation on the surface of Mercury, *Icarus*, *166*(2), 229–237, doi:10.1016/j.icarus.2003.08.005.

McPherron, R. L. (2005), Magnetic pulsations: Their sources and relation to solar wind and geomagnetic activity, *Surveys Geophys.*, *26*, 545–592, doi:10.1007/s10712-005-1758-7.

Miura, A. (1992), Kelvin-Helmholtz instability at the magnetospheric boundary: Dependence on the magnetosheath sonic Mach number, *J. Geophys. Res.*, *97*, 10,655–10,675.

Ness, N. F., K. W. Behannon, R. P. Lepping, and Y. C. Whang (1975), The magnetic field of Mercury, *J. Geophys. Res.*, *80*, 2708–2716.

Pantellini, F. G. E., D. Burgess, and S. J. Schwartz (1995), On the non-linear mirror instability, *Adv. Space Sci.*, *15*, 341–344.

Passot, T., and P. L. Sulem (2006), A fluid model with finite Larmor radius effects for mirror mode dynamics, *J. Geophys. Res.*, *111*, A04203, doi:10.1029/2005JA011425.

Russell, C. T., and M. M. Hoppe (1983), Upstream waves and particles, *Space Sci. Rev.*, *34*, 155–172.

Schwartz, S. J., D. Burgess, and J. J. Moses (1996), Low-frequency waves in the Earth's magnetosheath: present status, *Ann. Geophys.*, *14*, 1134–1150.

Sckopke, N. (1995), Ion heating at the Earth's quasi-perpendicular bow shock, *Adv. Space Sci.*, *15*(8-9), 261–269, doi:10.1016/0273-1177(94)00106-B.

Sckopke, N., G. Paschmann, S. J. Bame, J. T. Gosling, and C. T. Russell (1983), Evolution of Ion Distributions Across the Nearly Perpendicular Bow Shock: Specularly and Non-Specularly Reflected-Gyrating Ions, *J. Geophys. Res.*, *88*(A8), 6121–6136, doi:10.1029/JA088iA08p06121.

Slavin, J. A., et al. (2008), Mercury's magnetosphere after MESSENGER's first flyby, *Science*, *321*, 85–89.

Soucek, J., E. Lucek, and I. Dandouras (2008), Properties of magnetosheath mirror modes observed by Cluster and their responses to changes in plasma parameters, *J. Geophys. Res.*, *113*, A04203, doi:10.1029/2007JA012649.

Southwood, D. J., and M. G. Kivelson (1993), Mirror instability: 1. physical mechanism of linear instability, *J. Geophys. Res.*, *98*, 9181–9187.

Sundberg, T., S. a. Boardsen, J. a. Slavin, B. J. Anderson, H. Korth, T. H. Zurbuchen, J. M. Raines, and S. C. Solomon (2012), MESSENGER orbital observations of large-amplitude Kelvin-Helmholtz waves at Mercury's magnetopause, *J. Geophys. Res.*, *117*, 1–11, doi:10.1029/2011JA017268.

Taroyan, Y., and R. Erdélyi (2002), Resonant and Kelvin-Helmholtz instabilities on the magnetopause, *Phys. Plasmas*, *9*, 3121–3129.

Tatrallyay, M., G. Erdos, a. Balogh, and I. Dandouras (2008), The evolution of mirror type magnetic fluctuations in the magnetosheath based on multipoint observations, *Adv. Space Sci.*, *41*, 1537–1544.

Trávníček, P., P. Hellinger, and D. Schriver (2007a), Structure of Mercury's magnetosphere for different pressure of the solar wind: Three dimensional hybrid simulations, *Geophysical Research Letters*, *34*(5), 1–5, doi:10.1029/2006GL028518.

Trávníček, P. M. and Hellinger, P. and Schriver, D. and Herčík, D. and Slavin, J. A. and Anderson, B. J.(2009),Kinetic instabilities in Mercury's magnetosphere: Threedimensional simulation results, *Geophysical Research Letters*, *36*(7),1–5, doi: 10.1029/2008GL036630.

Trávníček, P., P. Hellinger, M. G. G. T. Taylor, C. P. Escoubet, I. Dandouras, and E. Lucek (2007b), Magnetosheath plasma expansion: Hybrid simulations, *Geophysical Research Letters*, *34*(15), 2–5, doi:10.1029/2007GL029728.

Trávníček, P. M., D. Schriver, P. Hellinger, D. Hercik, B. J. Anderson, M. Sarantos, and J. A. Slavin (2010), Mercury's magnetosphere-solar wind interaction for northward and southward interplanetary magnetic field: Hybrid simulation results, *Icarus*, *209*, 11–22.

Tsurutani, B. T., E. J. Smith, R. R. Anderson, K. W. Ogilvie, J. D. Scudder, D. N. Baker, and S. J. Bame (1982), Lion roars and nonoscillatory drift mirror waves in the magnetosheath, *J. Geophys. Res.*, *87*, 6060–6072.

Tsurutani, B. T., E. Echer, O. P. Verkhoglyadova, G. S. Lakhina, and F. Guarnieri (2011), Mirror instability upstream of the termination shock (ts) and in the heliosheath, *J. Atmos. Solar-Terrestrial Phys.*, *73*, 1398–1404, doi: 10.1016/j.jastp.2010.06.007.

Violante, L., M. B. Bavassano-Cattaneo, D. Moreno, and J. D. Richardson (1995), Observations of mirror waves and plasma depletion layer upstream of Saturn's magnetopause, *J. Geophys. Res.*, *100*, 12,047–12,055.

Walker, S. N., M. A. Balikhin, and M. Dunlop (2002), Mirror, structures in the magnetosheath: 3D structures or plane waves, *Adv. Space Sci.*, *30*, 2745–2750.

Yumoto, K. (1988), External and internal sources of low-frequency mhd waves in the magnetosphere - a review, *J. Geomag. Geoelectr.*, *40*, 293–311.

Zwan, B. J., and R. A. Wolf (1976), Depletion of solar wind plasma near a planetary boundary, *J. Geophys. Res.*, *81*, 1636.

P. Hellinger, Astronomical Institute & Institute of Atmospheric Physics, AS CR, Bocni II/1401, Prague 14131, Czech Republic. (petr.hellinger@asu.cas.cz)

David Herčík, Astronomical Institute & Institute of Atmospheric Physics, Academy of Sciences of the Czech Republic and Faculty of Nuclear Sciences and Physical Engineering, Czech Technical University, Prague, CR (hercik@asu.cas.cz)

Eun-Hwa Kim and Jay R. Johnson, Princeton Plasma Physics Laboratory, Princeton University, Princeton, NJ, USA

Pavel Trávníček, Space Sciences Laboratory, University California Berkeley, USA and Astronomical Institute & Institute of Atmospheric Physics, Academy of Sciences of the Czech Republic (AsI, ASCR)

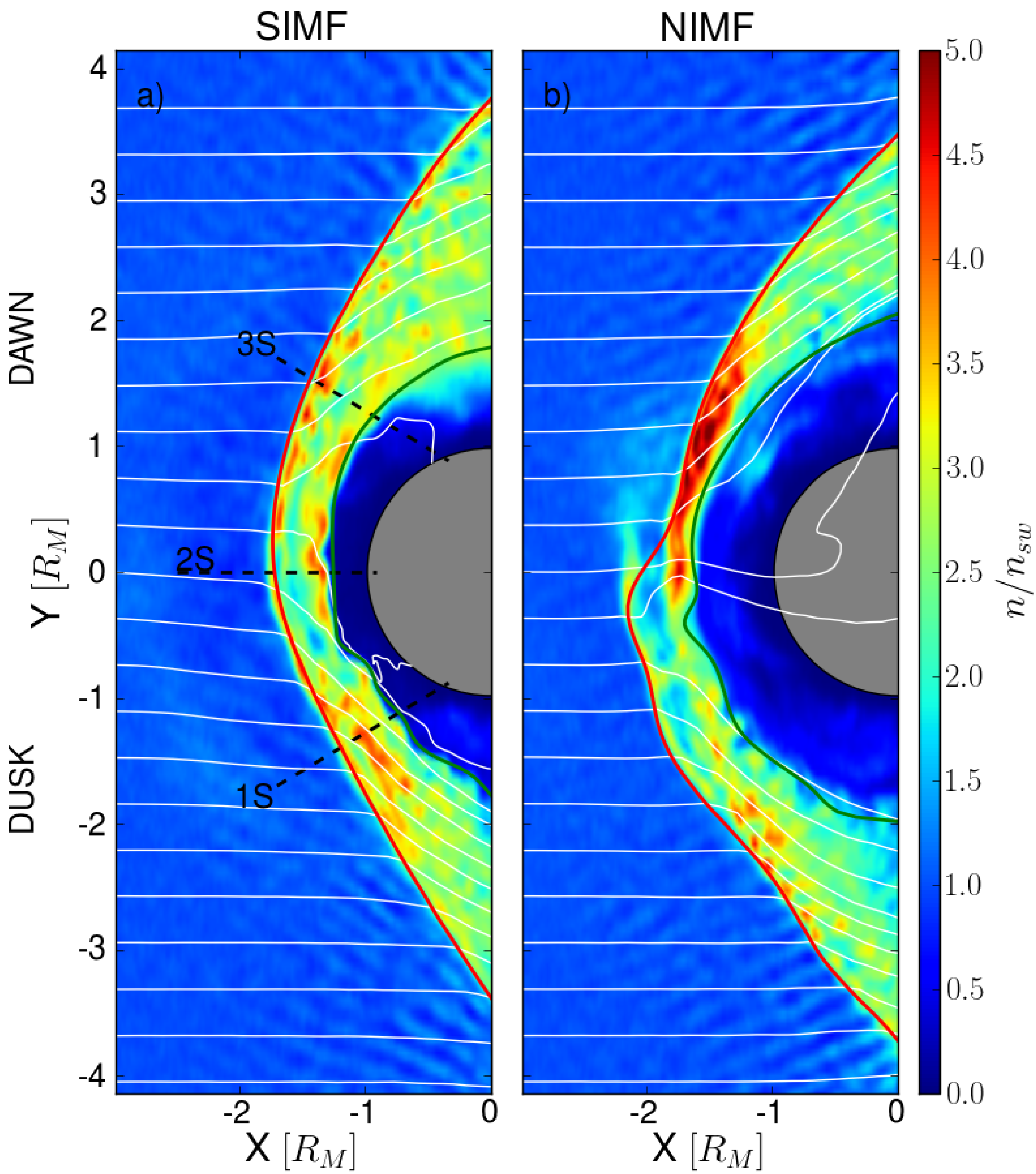

Figure 1. Color plots of proton density at the magnetic equator plane (0.2 R_M of the geographic equator plane). Panel a) shows data from the simulation SIMF and panel b) from the simulation NIMF. White solid lines show a projection of 3D flowlines started at the displayed plane -3 R_M ahead of the planet. The red solid line indicates a bow shock boundary and the green line indicates a magnetopause. The black dashed lines are virtual paths for further use later in the text.

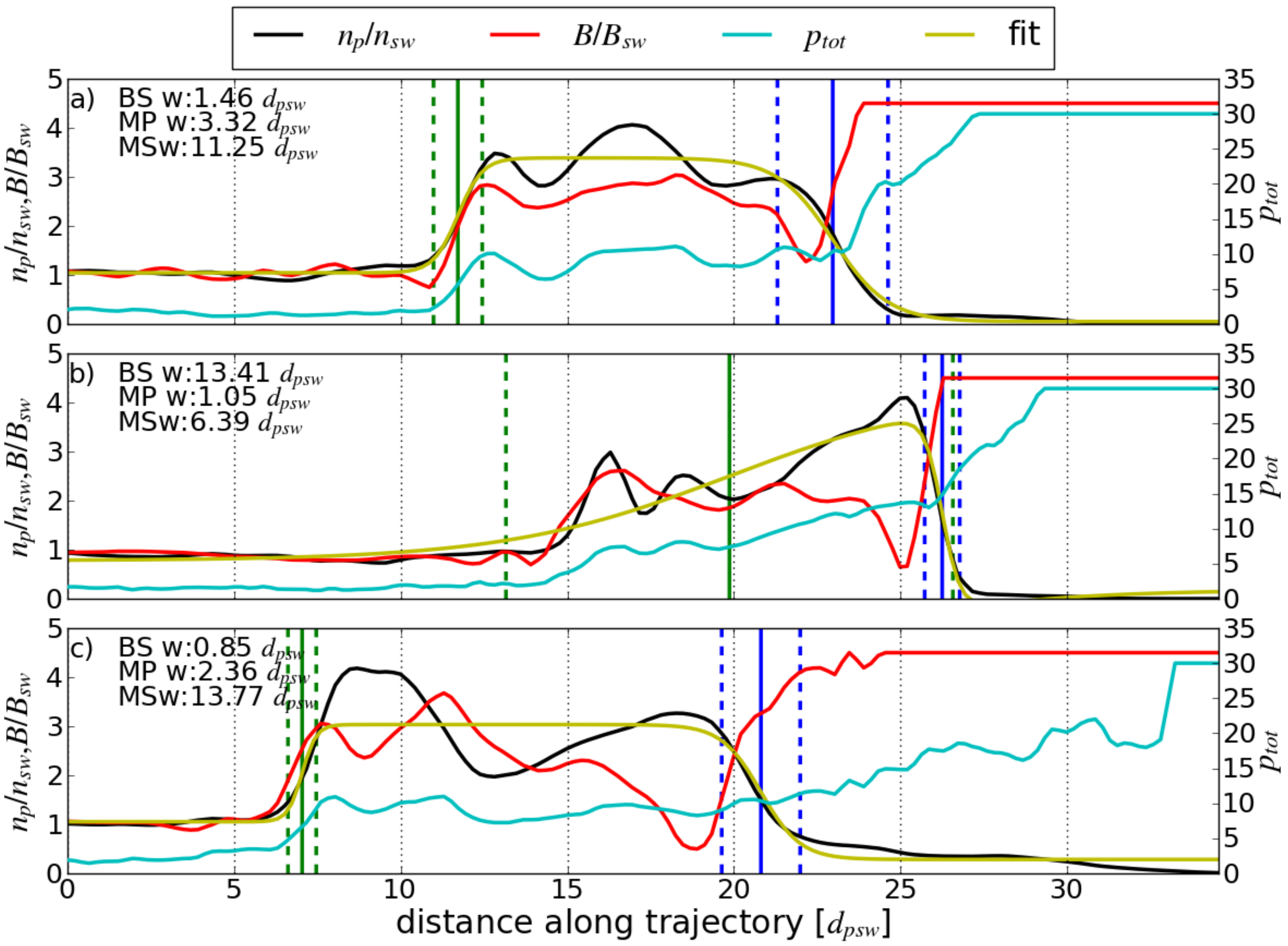

Figure 2. Data along virtual paths through datasets from SIMF as displayed in the Figure 1 on the left. Panel a) shows data for the trajectory 1S, panel b) for the trajectory 2S, and panel c) for 3S. All display proton density, magnetic field, and total pressure (plasma + magnetic) along the selected trajectory. All variables are normalized to the solar wind values, i.e. $n_{\mathrm{sw}}, B_{\mathrm{sw}}$, and plasma pressure p_{sw}. The magnetic field values are trimmed at 4.5 value and for total pressure at 30. Furthermore a fit of density data using function (3) is given. Based on the fit, positions of a bow shock and a magnetopause are indicated by the green and the blue solid vertical lines with estimated width of the boundary by dashed lines with respective colour. An estimated width of a bow shock, a magnetopause and a magnetosheath are given in proton inertial lengths in the solar wind d_{psw}.

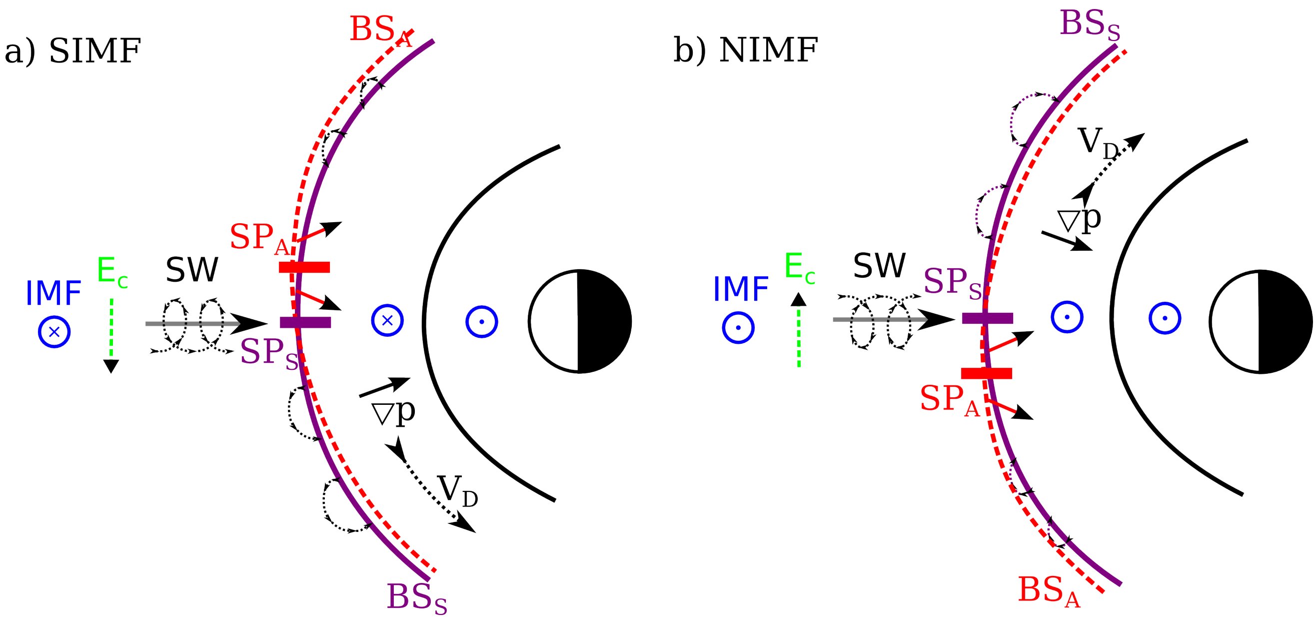

Figure 3. Sketch of processes leading to an asymmetric magnetosheath. Panel a) shows the configuration in the case of purely southward IMF and panel b) for northward IMF. *Legend*:E_c - Convective electric field, SW - Solar wind flow, BS_S - Symmetric bow shock, BS_A - Asymmetric bow shock, SP_S - Symmetric stagnation point, SP_A - Asymmetric stagnation point, V_D - Total drift direction, ∇P - Total pressure gradient, $\odot$ - Magnetic field pointing up, $\otimes$ - Magnetic field pointing down.

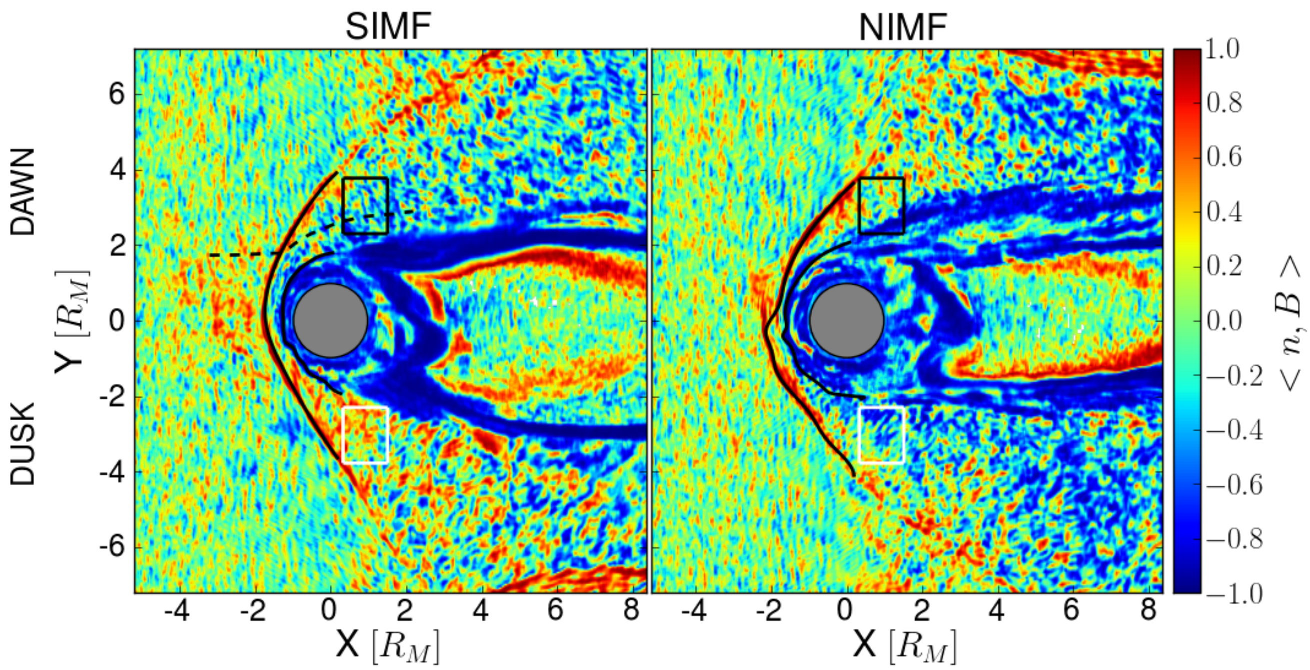

Figure 4. Colour scale plots of a correlation $\langle n_p, B\rangle$ for the simulation SIMF (southward IMF) left panel and NIMF (northward IMF) on the right. The plots are given in the magnetic equatorial plane (0.2 R_M above the equatorial plane towards the north pole). The black solid lines indicate an estimated bow shock and a magnetopause locations. Two magnetosheath regions indicated by the black (dawn) and the white (dusk) rectangles are for further reference as well as flowline shown in the black dashed line.

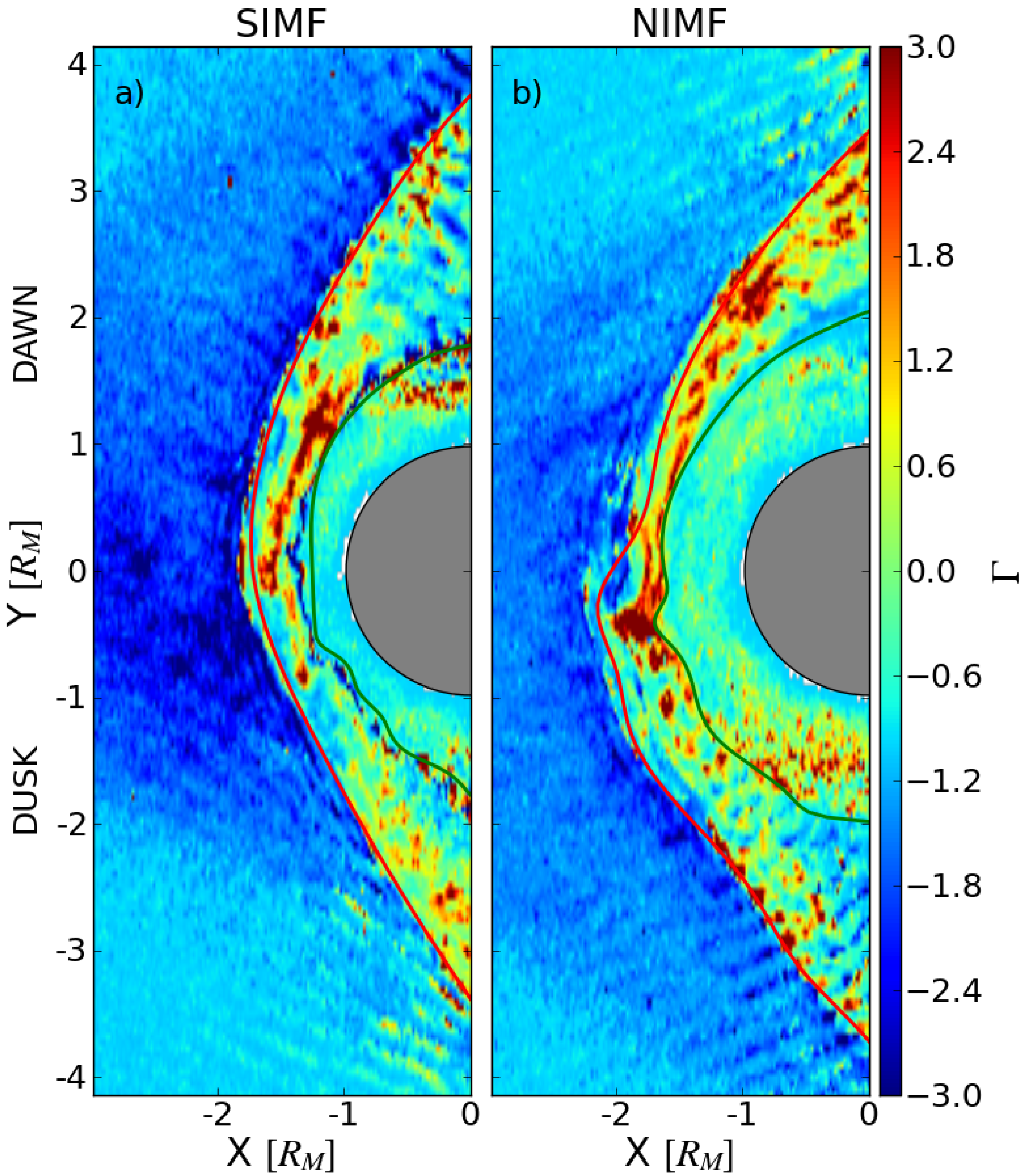

Figure 5. Colour scale plots of Γ in the magnetosheath for the simulation SIMF on the left and for NIMF on the right. Data plotted in the magnetic equator plane with estimated location of a bow shock (red line) and a magnetosheath (green line).

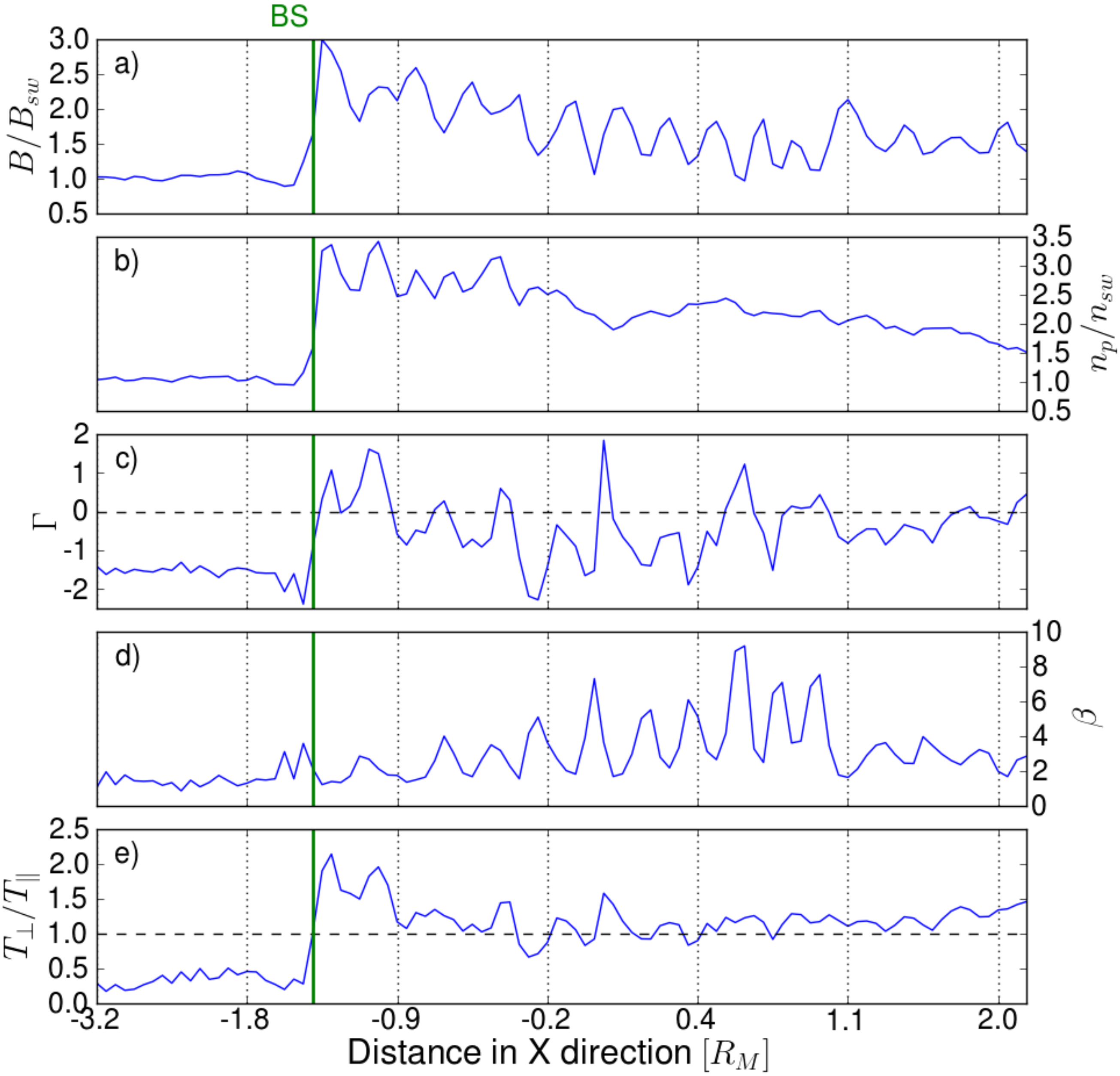

Figure 6. Data from the SIMF simulation along a flowline crossing the dawn region suspected of mirror waves. The flowline is indicated in the Figure 5 by the black dashed line. Panel a) gives a magnetic field amplitude normalized to the solar wind magnetic field, panel b) proton density normalized to the solar wind density, panel c) Γ, panel d) *beta*, and panel d) temperature anisotropy. The green solid vertical line denotes the position of a bow shock.

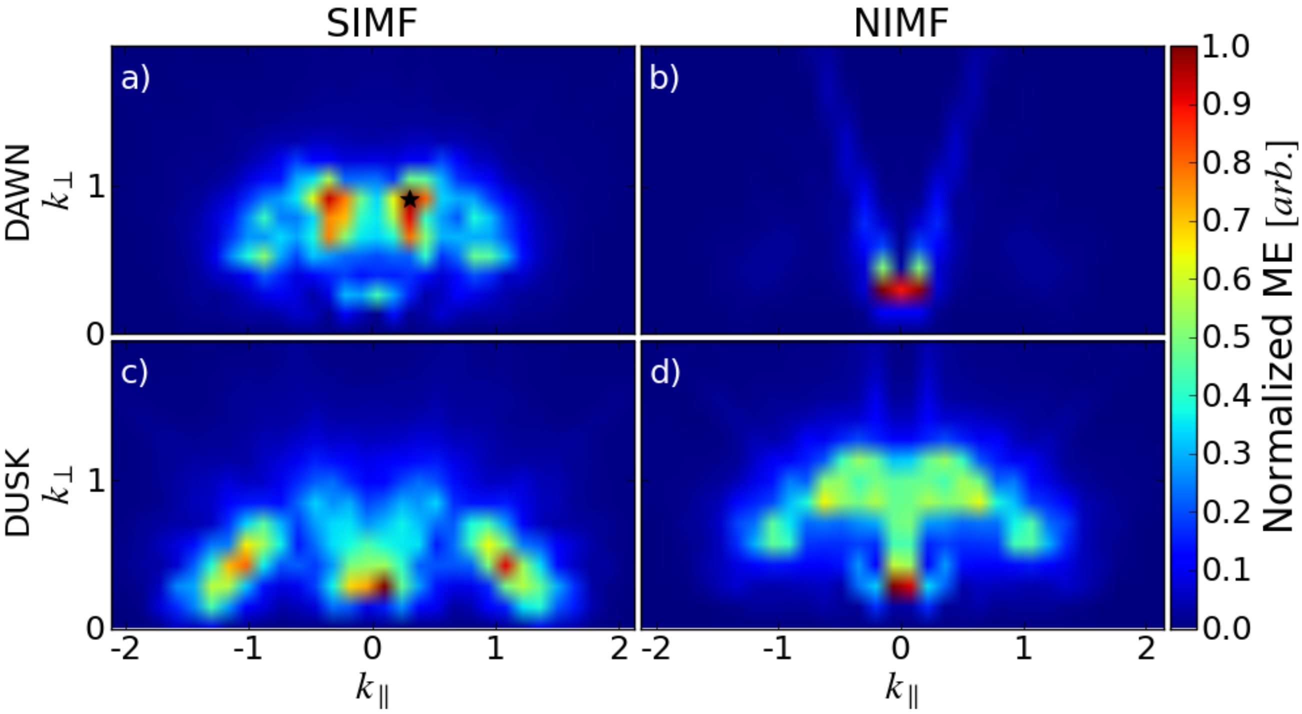

Figure 7. Results from spatial Fourier analysis of a magnetic fluctuation δB from selected regions of the two different simulations. Colour scale plots of δB^2 as a function of $k_\parallel$ and $k_\perp$ for the southward IMF (SIMF) simulation for the dawn (panel a)) and the dusk (panel c)) region. Results for the same analysis and region but for the northward IMF (NIMF) simulation show panels b) (for the dawn side) and d) (for the dusk side). The colour scale is normalized magnetic energy in arbitrary units. A star denotes main local maxima at the panel a).